Analytical model for characterizing the pear-shaped tribotest for tube hydroforming. Part 1

G Ngaile* and **C Yang**
Department of Mechanical and Aerospace Engineering, North Carolina State University, Raleigh, North Carolina, USA

Abstract: An analytical model to characterize the pear-shaped tribotest is presented. In this test, a tubular specimen is pressurized, forcing the material to flow towards the apex of a pear-shaped die. The height of the pear-shaped tube is a function of the magnitude of friction stress at the tube–die interface. Through a mechanistic approach, a closed-form solution for field variables die–tube contact pressure, effective stress/strain, longitudinal stress/strain, and hoop stress/strain can be computed as a function of input pressure loading. The model has been validated by finite element analysis. The closed-form solution can be used rapidly to establish the calibration curves for determination of friction coefficient in the pear-shaped tribotest. Of equal importance, the analytical model can be used to optimize both process and die geometric variables to suit specific needs such as die wear studies through monitoring local interface pressure loading, types of material to be tested, tube sizes, and so on. Details on the applications of the developed analytical model can be found in Part 2 of this paper.

Keywords: tribotest, friction coefficient, tube hydroforming, closed-form equations

1 INTRODUCTION

In recent years, the tube hydroforming (THF) process has received increased attention in the automotive and aerospace industries owing to its numerous advantages over stamped and welded assemblies. The advantages of THF include high strength-to-weight ratio, dimensional accuracy, and part consolidation [1–6]. In THF, a tubular blank is formed within a die cavity by forcing pressurized fluid inside so that the blank expands into the final shape. The coordination of inside pressure and feeding of the material by pushing the tube ends is critical to the success of the process. The drawback of this process is the longer cycle time. To make it competitive with other manufacturing processes, much research has been put into improving cycle time by developing new hydroforming press designs [7].

Tribology is also critical to the advancement of THF. Ineffective lubrication in THF can result in poor surface quality of the part: excessive friction

forces may impede optimal material flow to the die cavity, resulting in the formation of wrinkles or other defects that make a part unacceptable.

Typically, THF can be divided into three friction zones: guiding zone, transition zone, and expansion zone [8, 9]. Figure 1 shows an example of THF parts and friction zone categories. The guiding zone is where the material is pushed towards the die cavity to supply material. At the expansion zone, the material is forced to conform to the die cavity by the internal fluid pressure.

Owing to variation in punch velocities and the internal pressure loading, the material flow patterns may be complex, leading to severe tribological conditions at the tool-workpiece interface. Furthermore, the state of stress at the respective friction zones may differ considerably; the state of stress in the guiding zone is predominantly compression – leading to wall thickening – while in the expansion zone, the stress is predominantly tensile – leading to surface expansion and wall thinning. The differing tribological conditions suggest different lubrication mechanisms [8]. Previous studies have shown that lubricants that perform well in the guiding zone do not perform well in the expansion zone. This is attributed to differences in tribological conditions in the respective

*Corresponding author: Department of Mechanical and Aerospace Engineering, North Carolina State University, Campus Box 7910, Raleigh, NC 27695, USA. email: gracious_ngaile@ncsu.edu; gngaile@eos.ncsu.edu
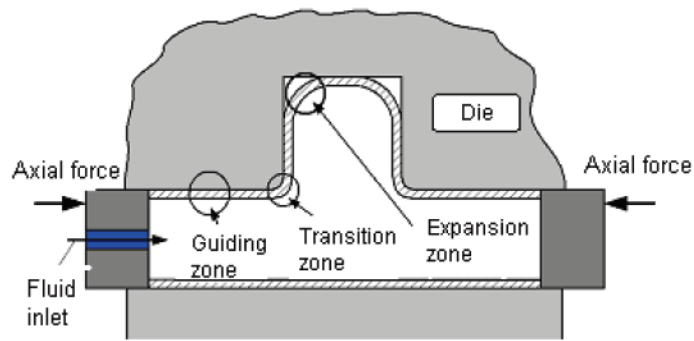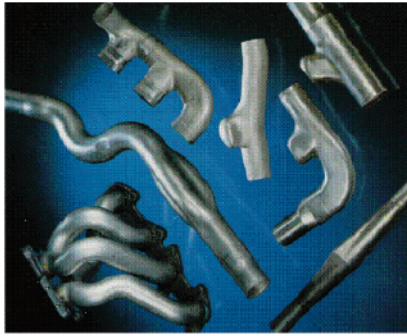
Fig. 1 Sample THF part and friction zone

zones. Lubricant developers are attempting to devise effective lubrication in THF [10].

Tribotests that mimic tribological conditions in THF are critical for evaluating candidate lubricants. Two commonly used tribotests to evaluate lubricants for the expansion zone are the corner fill test, which was originally developed by the Industrial Research and Development Institute (IRDI) in Canada [11], and the pear-shaped expansion test, which was developed at the Ohio State University [8, 12]. Figures 2(a) and (b) show the corner fill and pear-shaped expansion tests, respectively. The premise behind the corner fill test is that under good lubrication conditions, the tube will be inflated to tight corner radii before fracture and the wall thickness distribution will be uniform. In the case of higher friction at the tube–die interface, fracture will occur prematurely or significant wall thinning will be observed near the corner [11].

While in the corner fill test, material flows towards all four corners, the pear-shaped expansion test confines the material to flow in one direction only. After expanding the tube to pressure Pi, δ or protrusion height PH can be determined. PH is the distance from the bottom of the tube to the apex. Delta at fracture δf is a function of friction stress τ_s, flow stress, σ, and internal pressure Pi. The die angle ψ can be optimized via numerical modelling by maximizing the difference between $\delta^{\mu 2}$ and $\delta^{\mu 1}$. Performance evaluation of the lubricants can be achieved based on three criteria: wall thinning distribution – the lower the wall thinning, the better the lubricant; protrusion height PH – the higher the height of protrusion, the better the lubricant; and bursting pressure – the higher the bursting pressure, the better the lubricant [12].

Although these tests can effectively be used in ranking lubricant performance, the friction coefficient for the lubricant tested cannot be determined directly. Friction values are important for process modelling via computer simulation. Obtaining friction coefficients

experimentally from these tests is complicated, if not impossible, because of the geometric constraints that prohibit placement of load cells. One way to obtain apparent friction coefficients is to combine experiments and numerical modelling via finite element analysis (FEA); however, this is time consuming. There is a need for analytical solutions for friction characterization in the expansion zone.

OBJECTIVES AND APPROACH

The goal of this paper is to develop a closed-form solution that will provide ways to determine the state of stress and strain along a deforming pear shape that is subjected to internal pressure Pi. The specific objectives are as follows:

(a) develop a mathematical model that will provide the interface pressure distribution around the deforming tube as a function of the internal pressure;

(b) establish mathematical relationships that encompass principal stresses, strains, material parameters, and geometric variables (tube and die) that will facilitate optimization of the pear-shaped tribotest, i.e. obtaining pear-shaped geometry that is friction sensitive for use in materials with different formability levels;

(c) derive mathematical relationships that can be used to establish friction calibration curves.

The authors expect that the analytical models will benefit both tribologists and THF process designers, as models will quickly provide better understanding of the local loads transmitted to the die systems, particularly for parts similar to pear shape. Also, capturing pressure distribution will provide information on die areas with peak pressures that may need special attention to suppress die wear.

The derivation commences by subdividing the pear shape into three sections: circular section, linear

section, and free section, as shown in Fig. 3. Balance of forces is taken at each section to establish the relationships between radial stresses σ_r, hoop stresses σ_θ, and longitudinal stresses σ_z. The flow stress used is assumed to obey von Mises yield criteria and the power law $\sigma = K\varepsilon^n$. The pear shape is assumed to be long enough to satisfy plane strain condition, that is, $\varepsilon_z = 0$. The remaining principal strains are derived in all sections, after which boundary conditions are invoked and the final equations are solved for the unknown variables using the Newton–Raphson method.

The major assumptions used in the analysis are:

(a) the longitudinal strain is ignored; therefore, the tube is assumed to be in plane strain state during the deformation;

(a)

Fig. 2(a) Corner fill test

(b) the tube is subdivided into three deforming sections: arc section, linear section, and free expansion section;

(c) the deformed shape at the free expansion section is assumed to be an arc;

(d) the tube is considered to be a thin wall structure, and hoop stress is assumed to be uniform through the thickness;

(e) the hoop stress is continuous along the hoop direction.

3 STRESS AND STRAIN ANALYSIS

3.1 Arc section

3.1.1 Stress analysis

Figure 4 shows the arc section where a summation of forces is taken with respect to an element cut from the arc section.

Taking summation of forces in the hoop direction, the following can be obtained

$$\sigma_\theta(\theta + d\theta)t - \sigma_\theta(\theta)t - \sigma_f r \, d\theta = 0$$

$$\frac{d\sigma_\theta}{d\theta} = \frac{r}{t}\sigma_f$$

$$\sigma_f = \mu|\sigma_r|$$

Note that the absolute symbol is used to guarantee that the friction stress is positive

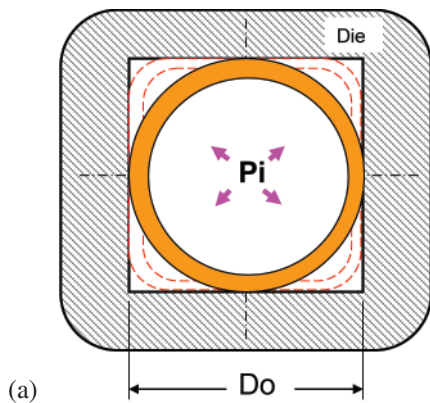$$\frac{d\sigma_\theta}{d\theta} = \frac{r\mu}{t}|\sigma_r| \tag{1}$$
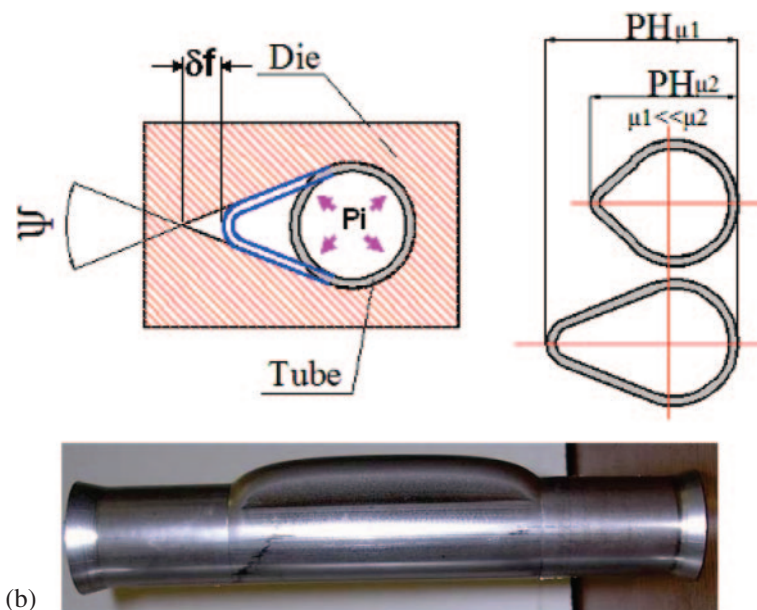

(b)
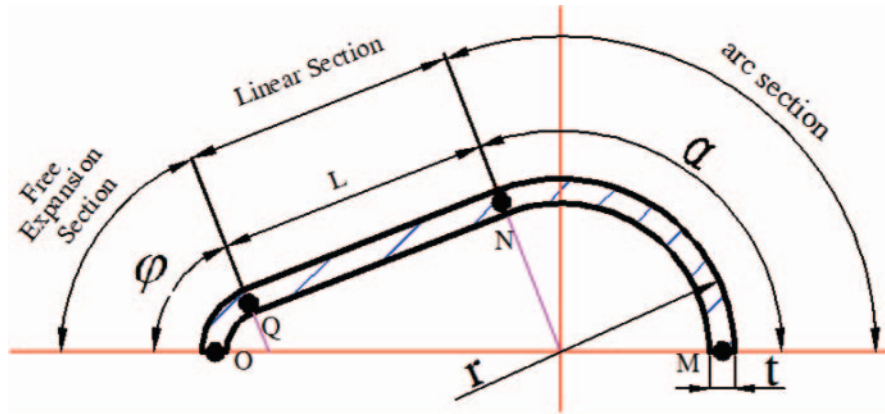
Fig. 2(b) Pear-shaped expansion test

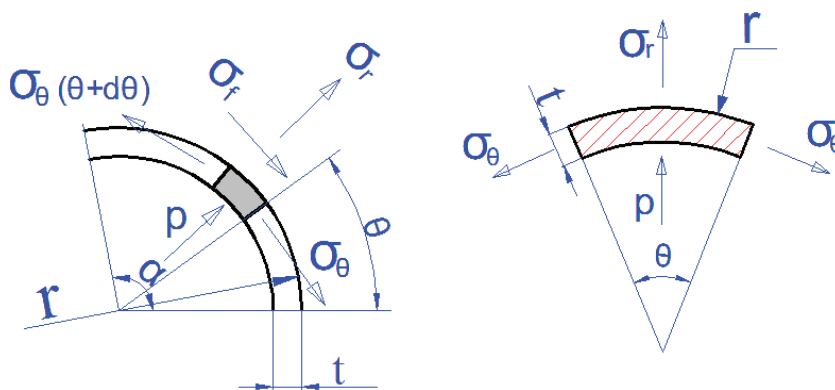**Fig. 3**   Three sections of deformed shape in half tubular model

Fig. 4   Stresses acting on arc section element

The summation of forces in the radial direction leads to

$$pA_1 + \sigma_r A_2 - 2\sigma_\theta A_3 \sin\frac{\theta}{2} = 0$$

$$\begin{cases} A_1 = (r - t)\theta \\ A_2 = r\theta \\ A_3 = t \end{cases}$$

$$p(r - t)\theta + \sigma_r r\theta - 2\sigma_\theta t \sin\frac{\theta}{2} = 0$$

As $\theta \to 0$, $\lim\limits_{\theta \to 0} 2 \sin\frac{\theta}{2} = \theta$

$$p(r - t)\theta + \sigma_r r\theta - \sigma_\theta t\theta = 0$$

$$\sigma_r = -\frac{p(r - t) - \sigma_\theta t}{r} \tag{2}$$

Under plane strain condition, the longitudinal strain is zero. Using Hencky's Total Deformation theory [13], the balance equation in the longitudinal direction leads to equation (3). Thus, from equations (1), (2), and (3), equation group (4) is obtained. This equation describes the interrelationships of stresses in the arc section

$$\varepsilon_z = \frac{d\bar{\varepsilon}}{d\bar{\sigma}}(\sigma_z - (\sigma_\theta + \sigma_r)/2) = 0$$

$$\sigma_z = (\sigma_\theta + \sigma_r)/2 \tag{3}$$

$$\begin{cases} \dfrac{d\sigma_\theta}{d\theta} = \dfrac{r\mu}{t}|\sigma_r| \\ \sigma_r = -\dfrac{p(r - t) - \sigma_\theta t}{r} \\ \sigma_z = (\sigma_\theta + \sigma_r)/2 \end{cases} \tag{4}$$

3.1.2   Effective stress and strain under plane strain conditions

Assuming von Mises yield criterion, effective stress can be represented by equation (5). By substituting equation (3) into equation (5), the effective stress under plane strain conditions is obtained as given in equation (7)

$$\bar{\sigma} = \frac{1}{\sqrt{2}}\sqrt{(\sigma_z - \sigma_r)^2 + (\sigma_r - \sigma_\theta)^2 + (\sigma_\theta - \sigma_z)^2} \tag{5}$$

$$\bar{\sigma} = \frac{\sqrt{3}}{2}\sqrt{(\sigma_\theta - \sigma_r)^2} \tag{6}$$

$$\bar{\sigma} = \frac{1}{\beta}(\sigma_\theta - \sigma_r) \quad \beta = \frac{2}{\sqrt{3}} \tag{7}$$

Effective strain is expressed by equation (8). Owing to the plane strain condition, the longitudinal strain ε_z

equals 0, as shown in equation (9). Substituting equation (9) into equation (8) and considering a positive hoop strain ε_θ, equation (10) is obtained

$$\bar{\varepsilon} = \frac{\sqrt{2}}{3}\sqrt{(\varepsilon_z - \varepsilon_r)^2 + (\varepsilon_r - \varepsilon_\theta)^2 + (\varepsilon_\theta - \varepsilon_z)^2} \qquad (8)$$

$$\begin{cases} \varepsilon_z = 0 \\ \varepsilon_\theta + \varepsilon_r = 0 \end{cases} \qquad (9)$$

$$\bar{\varepsilon} = \frac{2}{\sqrt{3}}\sqrt{\varepsilon_\theta^2}$$

$$\bar{\varepsilon} = \beta\varepsilon_\theta \qquad \beta = \frac{2}{\sqrt{3}} \qquad (10)$$

The power law will be used to formulate the relation between effective stress and effective strain as given by equation (11). By substituting equations (7) and (10) into equation (11), equations (12) and (13) can be obtained

$$\bar{\sigma} = K\bar{\varepsilon}^n \qquad (11)$$

$$\frac{1}{\beta}(\sigma_\theta - \sigma_r) = K\beta^n \varepsilon_\theta^n \qquad (12)$$

$$\sigma_\theta - \sigma_r = K\beta^{n+1}\varepsilon_\theta^n \qquad (13)$$

Combining equation (13) and group equation (4), the following can be obtained

$$\begin{cases} \dfrac{d\sigma_\theta}{d\theta} = \dfrac{r\mu}{t}|\sigma_r| \\ \sigma_r = -\dfrac{p(r-t) - \sigma_\theta t}{r} \\ \sigma_z = (\sigma_\theta + \sigma_r)/2 \quad \sigma_\theta - \sigma_r = K\beta^{n+1}\varepsilon_\theta^n \end{cases} \qquad (14)$$

3.1.3 Derivation of strain in arc section

In this section, the expression for strain will be derived and also the stresses σ_θ, σ_r, σ_z will be expressed as function of strain. From equation (14), the following simultaneous equations can be solved for σ_θ and σ_r, with the results given in equations (15) and (16), respectively

$$\begin{cases} \sigma_r = -\dfrac{p(r-t) - \sigma_\theta t}{r} \\ \sigma_\theta - \sigma_r = K\beta^{n+1}\varepsilon_\theta^n \end{cases}$$

$$\sigma_\theta = \frac{K\beta^{n+1}\varepsilon_\theta^n - (r - t/r)p}{1 - t/r} \qquad (15)$$

$$\sigma_r = -\frac{(r - t/t)p - K\beta^{n+1}\varepsilon_\theta^n}{r/t - 1} \qquad (16)$$

From equation (15)

$$\frac{d\sigma_\theta}{d\theta} = \frac{d\{|-[K\beta^{n+1}\varepsilon_\theta^n - (r - t/r)p]/(1 - t/r)|\}}{d\theta}$$

$$= \frac{d\{K\beta^{n+1}\varepsilon_\theta^n - (r - t/r)p/(1 - t/r)\}}{d\theta}$$

$$\qquad (17)$$

The factors $1 - t/r$ and $r - t/r$ in equation (17) vary with θ, owing to the variation of thickness t with θ. But the variation is insignificant. Therefore, in the differential $d\sigma_\theta/d\theta$, these two factors are considered to be constant along the hoop direction

$$\frac{d\sigma_\theta}{d\theta} = \frac{K\beta^{n+1}n\varepsilon_\theta^{n-1}}{1 - t/r}\frac{d\varepsilon_\theta}{d\theta} \qquad (18)$$

Substituting equation (16) into equation (14), the following can be obtained

$$\begin{aligned} \frac{d\sigma_\theta}{d\theta} &= \frac{r\mu}{t}\left|-\frac{K\beta^{n+1}\varepsilon_\theta^n - (r - t/r)p}{1 - t/r}\right| \\ &= \frac{r\mu}{t}\frac{(r - t/t)p - K\beta^{n+1}\varepsilon_\theta^n}{r/t - 1} \end{aligned} \qquad (19)$$

Equating equations (18) and (19)

$$\frac{K\beta^{n+1}n\varepsilon_\theta^{n-1}}{1 - t/r}\frac{d\varepsilon_\theta}{d\theta} = \frac{r\mu}{t}\frac{(r - t/t)p - K\beta^{n+1}\varepsilon_\theta^n}{r/t - 1}$$

$$\frac{K\beta^{n+1}n\varepsilon_\theta^{n-1}}{1 - t/r}\frac{d\varepsilon_\theta}{d\theta} = \mu\frac{(r - t/t)p - K\beta^{n+1}\varepsilon_\theta^n}{1 - t/r}$$

$$K\beta^{n+1}n\varepsilon_\theta^{n-1}\frac{d\varepsilon_\theta}{d\theta} = \frac{r - t}{t}\mu p - \mu K\beta^{n+1}\varepsilon_\theta^n \qquad (20)$$

Although r/t can vary along the arc section owing to variation of wall thickness t, the variation is assumed to be insignificant. Thus $\lambda = \frac{r}{t} \approx \frac{r}{t_0}$

$$K\beta^{n+1}n\varepsilon_\theta^{n-1}\frac{d\varepsilon_\theta}{d\theta} = (\lambda - 1)\mu p - \mu K\beta^{n+1}\varepsilon_\theta^n \qquad (21)$$

$$\begin{cases} a = K\beta^{n+1} \\ b = -\mu K\beta^{n+1} \\ c = (\lambda - 1)\mu p \end{cases} \qquad (22)$$

Substituting equation (22) into equation (21), equation (23) is obtained

$$an\varepsilon_\theta^{n-1}\frac{d\varepsilon_\theta}{d\theta} = b\varepsilon_\theta^n + c \qquad (23)$$

$$\int \frac{an\varepsilon_\theta^{n-1}d\varepsilon_\theta}{b\varepsilon_\theta^n + c} = \int d\theta$$

$$\frac{a}{b}\int \frac{d(b\varepsilon_\theta^n + c)}{b\varepsilon_\theta^n + c} = \int d\theta$$

$$\frac{a}{b}\ln(b\varepsilon_\theta^n + c) + c_0 = \theta \qquad (24)$$

The constant of integration c_0 can be obtained by substituting the boundary condition $\theta = \alpha$ and $\varepsilon_\theta = \varepsilon_N$. Where ε_N is the strain at intersection between the arc and linear sections, refer to Fig. 3

$$c_0 = \alpha - \frac{a}{b}\ln(b\varepsilon_N^n + c)$$

$$\theta - \alpha = \frac{a}{b}\ln\frac{(b\varepsilon_\theta^n + c)}{(b\varepsilon_N^n + c)}$$

$$\varepsilon_\theta = \left\{\left(\varepsilon_N^n + \frac{c}{b}\right)e^{b/a(\alpha-\theta)} - \frac{c}{b}\right\}^{1/n} \quad (25)$$

Substituting equation (22) into equation (25), equation (26) is obtained

$$\varepsilon_\theta = \left\{\frac{(\lambda-1)p}{K\beta^{n+1}} - \left[\frac{(\lambda-1)p}{K\beta^{n+1}} - \varepsilon_N^n\right]e^{\mu(\theta-\alpha)}\right\}^{1/n} \quad (26)$$

Substituting equation (26) into equations (15) and (16), the equations for σ_θ and σ_r can be obtained respectively. The equation for σ_z is obtained by substituting equations (27) and (28) into equation (3)

$$\sigma_\theta = \left(\frac{\lambda K\beta^{n+1}\varepsilon_N^n}{\lambda-1} - \lambda p\right)e^{\mu(\theta-\alpha)} + (\lambda-1)p \quad (27)$$

$$\sigma_r = -\left(p - \frac{K\beta^{n+1}\varepsilon_N^n}{\lambda-1}\right)e^{\mu(\theta-\alpha)} \quad (28)$$

$$\sigma_z = \frac{1}{2}\left\{\frac{(\lambda+1)}{\lambda-1}K\beta^{n+1}\varepsilon_N^n - (\lambda+1)p\right\}e^{\mu(\theta-\alpha)} + \frac{(\lambda-1)}{2}p \quad (29)$$

The relationships for the stress and strain for the arc section have now been derived as given in equation group (30)

$$\begin{cases} \sigma_\theta = \left(\frac{\lambda K\beta^{n+1}\varepsilon_N^n}{\lambda-1} - \lambda p\right)e^{\mu(\theta-\alpha)} + (\lambda-1)p \\ \sigma_r = -\left(p - \frac{K\beta^{n+1}\varepsilon_N^n}{\lambda-1}\right)e^{\mu(\theta-\alpha)} \\ \sigma_z = \frac{1}{2}\left[\frac{(\lambda+1)}{\lambda-1}K\beta^{n+1}\varepsilon_N^n - (\lambda+1)p\right]e^{\mu(\theta-\alpha)} + \frac{(\lambda-1)}{2}p \\ \varepsilon_\theta = \left\{\frac{(\lambda-1)p}{K\beta^{n+1}} - \left[\frac{(\lambda-1)p}{K\beta^{n+1}} - \varepsilon_N^n\right]e^{\mu(\theta-\alpha)}\right\}^{1/n} \\ \varepsilon_r = -\left\{\frac{(\lambda-1)p}{K\beta^{n+1}} - \left[\frac{(\lambda-1)p}{K\beta^{n+1}} - \varepsilon_N^n\right]e^{\mu(\theta-\alpha)}\right\}^{1/n} \\ \varepsilon_z = 0 \end{cases} \quad (30)$$

3.2 Linear section

3.2.1 Stress analysis of linear section

Figure 5 shows an element in the linear section where summation of forces is taken in the hoop and radial directions.

Equilibrium equation in the hoop direction

$$\sigma_\theta(x + dx)t - \sigma_\theta(x)t - \sigma_f dx = 0$$

$$\frac{d\sigma_\theta}{dx} = \frac{1}{t}\sigma_f$$

$$\sigma_f = \mu|\sigma_r|$$

$$\frac{d\sigma_\theta}{dx} = \frac{\mu}{t}|\sigma_r| \quad (31)$$
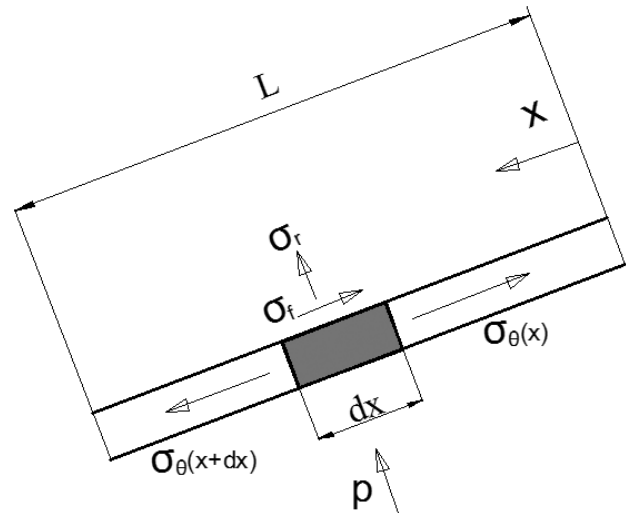

Fig. 5 Stress acting on an element in the linear section

Equilibrium equation in the radial direction $\sigma_r = -p$ From equation (31), the following equation group holds in the linear section

$$\begin{cases} \frac{d\sigma_\theta}{dx} = \frac{\mu}{t}|\sigma_r| \\ \sigma_r = -p \\ \sigma_z = (\sigma_\theta + \sigma_r)/2 \end{cases} \quad (32)$$

3.2.2 Derivation of strain in the linear section

The expressions for strain are derived and also the stress components as a function of strain are established. Combining equations (32) and (13), the following can be obtained

$$\begin{cases} \frac{d\sigma_\theta}{dx} = \frac{\mu}{t}|\sigma_r| \\ \sigma_r = -p \\ \sigma_z = (\sigma_\theta + \sigma_r)/2 \\ \sigma_\theta - \sigma_r = K\beta^{n+1}\varepsilon_\theta^n \end{cases} \quad (33)$$

From equation (33), the following equations can be derived

$$\begin{cases} \sigma_\theta = K\beta^{n+1}\varepsilon_\theta^n - p \\ \frac{d\sigma_\theta}{dx} = \frac{\mu}{t}p \end{cases} \quad (34)$$

$$\frac{d\sigma_\theta}{dx} = \frac{d(K\beta^{n+1}\varepsilon_\theta^n - p)}{dx}$$

$$\frac{d\sigma_\theta}{dx} = K\beta^{n+1}n\varepsilon_\theta^{n-1}\frac{d\varepsilon_\theta}{dx} \quad (35)$$

Substituting equation (35) into equation (34)

$$\frac{\mu}{t}p = K\beta^{n+1}n\varepsilon_\theta^{n-1}\frac{d\varepsilon_\theta}{dx} \quad (36)$$

$$t = t_0 e^{\varepsilon_r} = t_0 e^{-\varepsilon_\theta} \quad (37)$$

$$\frac{\mu}{t_0 \mathrm{e}^{-\varepsilon_\theta}} p = K\beta^{n+1} n \varepsilon_\theta^{n-1} \frac{\mathrm{d}\varepsilon_\theta}{\mathrm{d}x}$$

$$\frac{\mu}{t_0} p = K\beta^{n+1} n \varepsilon_\theta^{n-1} \mathrm{e}^{-\varepsilon_\theta} \frac{\mathrm{d}\varepsilon_\theta}{\mathrm{d}x} \tag{38}$$

$$\mathrm{e}^{-\varepsilon_\theta} = 1 + \sum_{i=1}^{\infty} \frac{(-1)^i (\varepsilon_\theta)^i}{i!}$$

$$\frac{\mu}{t_0} p = K\beta^{n+1} n \varepsilon_\theta^{n-1} \left[1 + \sum_{i=1}^{\infty} \frac{(-1)^i (\varepsilon_\theta)^i}{i!} \right] \frac{\mathrm{d}\varepsilon_\theta}{\mathrm{d}x} \tag{39}$$

$$\int \frac{\mu p}{K\beta^{n+1} n t_0} \mathrm{d}x = \int \left[1 + \sum_{i=1}^{\infty} \frac{(-1)^i (\varepsilon_\theta)^i}{i!} \right] \varepsilon_\theta^{n-1} \mathrm{d}\varepsilon_\theta \tag{40}$$

$$\frac{\mu p}{K\beta^{n+1} n t_0} x = \frac{1}{n} \varepsilon_\theta^n + \sum_{i=1}^{\infty} \frac{(-1)^i}{i!} \frac{1}{i+n} (\varepsilon_\theta)^{i+n} + c_0$$

Taking boundary conditions of $x = 0$ and $\varepsilon_\theta = \varepsilon_N$, c_0 can be obtained

$$c_0 = -\frac{1}{n} \varepsilon_N^n - \sum_{i=1}^{\infty} \frac{(-1)^i}{i!} \frac{1}{i+n} (\varepsilon_N)^{i+n} \tag{41}$$

$$\frac{1}{n} (\varepsilon_\theta^n - \varepsilon_N^n) + \sum_{i=1}^{\infty} \frac{(-1)^i}{i!} \frac{1}{i+n} (\varepsilon_\theta^{i+n} - \varepsilon_N^{i+n})$$
$$= \frac{\mu p}{K\beta^{n+1} n t_0} x \tag{42}$$

From equation (42) the average hoop strain ε_θ distribution for the linear section can be obtained. By substituting the hoop strain from equation (42) into equation (43) the state of stress and strain along the linear section can be determined

$$\begin{cases} \sigma_\theta = K\beta^{n+1} \varepsilon_\theta^n - p \\ \sigma_r = -p \\ \sigma_z = \frac{1}{2} K\beta^{n+1} \varepsilon_\theta^n - p \\ \varepsilon_r = -\varepsilon_\theta \\ \varepsilon_z = 0 \end{cases} \tag{43}$$

3.3 Free expansion section

3.3.1 Stress analysis of free expansion section

Figure 6 shows an element in the free expansion section where hoop stress is assumed to be constant and equal to hoop stress at the end of the linear section. The equilibrium relations are given in equation (44)

$$\begin{cases} \sigma_\theta = \sigma_Q \\ \sigma_r = 0 \\ \sigma_z = \frac{1}{2}(\sigma_\theta + \sigma_r) \end{cases} \tag{44}$$

3.3.2 Derivation of strain in free expansion section

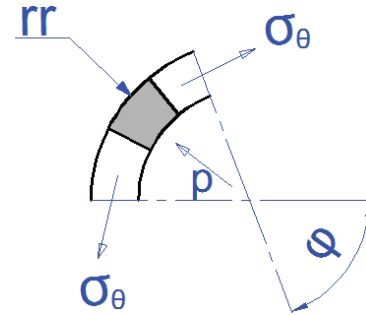In the free expansion section, average hoop strain is assumed to be constant and equal to hoop strain at

Fig. 6 Stress acting on an element in the free expansion sections

the end of the linear section. ε_Q can be calculated from equation (42) by substituting the boundary conditions $x = L$ and $\varepsilon_\theta = \varepsilon_Q$, which leads to equation (45)

$$\frac{1}{n} (\varepsilon_Q^n - \varepsilon_N^n) + \sum_{i=1}^{\infty} \frac{(-1)^i}{i!} \frac{1}{i+n} (\varepsilon_Q^{i+n} - \varepsilon_N^{i+n})$$
$$= \frac{\mu p}{K\beta^{n+1} n t_0} L \tag{45}$$

By substituting the hoop strain ε_Q from equation (45) into equation (46) the state of stress and strain in the free expansion section can be determined

$$\begin{cases} \sigma_\theta = K\beta^{n+1} \varepsilon_Q^n \\ \sigma_r = 0 \\ \sigma_z = \frac{1}{2} K\beta^{n+1} \varepsilon_Q^n \\ \varepsilon_\theta = \varepsilon_Q \\ \varepsilon_r = -\varepsilon_Q \\ \varepsilon_z = 0 \end{cases} \tag{46}$$

Equations (30), (43), and (46) provide average stress and strain values in the arc, linear, and free expansion sections. That is, the average stress and strain values exhibited at the middle layer of the tube. It should be noted that at the linear and free expansion sections, the tubular material exhibits bending and unbending as the material flows to the die corner. Therefore the state of stress and strain in the inner tube layer will be different from the outer tube layer. Additional derivations for the inner and outer layer are given in Appendix 2.

4 ESTABLISHMENT OF BOUNDARY CONDITIONS

4.1 Boundary condition calculation

From the above analysis, the stress and strain in the three sections are solved and expressed in explicit equations. But the boundary condition ε_N is involved in the equations of the linear section and the arc section. Before calculating stress and strain distribution, ε_N should be solved for first. ε_N can be obtained by the constant volume condition. Before deformation,

the volume of the tube with unit longitudinal distance can be expressed by equation (47), taking one half of the tube section

$$V_0 = \pi r t \tag{47}$$

The volume after deformation can be calculated as

$$V = \int_0^{st} t \, ds \tag{48}$$

where st is the curvilinear length of the deformed tube and t is the thickness of the deformed tube

$$V = V_0 \tag{49}$$

The volume of the arc section can be calculated as follows

$$V_c = \int_0^{\alpha} tr \, d\theta$$

$$\varepsilon_\theta = \ln \frac{t_0}{t} \quad \Rightarrow \quad t = t_0 e^{-\varepsilon_\theta}$$

$$V_c = \int_0^{\alpha} r t_0$$

$$\times e^{-\left(\left\{\varepsilon_N^n - \left[(\lambda-1)p/K\beta^{n+1}\right]\right\} e^{b/a(\theta-\alpha)} + \left[(\lambda-1)p/K\beta^{n+1}\right]\right)^{1/n}} d\theta \tag{50}$$

The volume of the linear section can be calculated as follows

$$V_L = \int_0^L t \, dx$$

$$= \int_0^L t_0 e^{-\varepsilon_\theta} \, dx$$

From equation (39)

$$dx = \frac{t_0}{p\mu} K\beta^{n+1} n \varepsilon_\theta^{n-1} e^{\varepsilon_\theta} d\varepsilon_\theta$$

$$V_L = \int_0^L t_0 e^{-\varepsilon_\theta} \, dx$$

$$V_L = \int_{\varepsilon_N}^{\varepsilon_Q} t_0 e^{-\varepsilon_\theta} \left\{ \frac{t_0}{p\mu} K\beta^{n+1} n \varepsilon_\theta^{n-1} e^{-\varepsilon_\theta} d\varepsilon_\theta \right\}$$

$$V_L = \frac{(t_0)^2 K\beta^{n+1}}{p\mu} \int_{\varepsilon_N}^{\varepsilon_Q} n \varepsilon_\theta^{n-1} e^{-2\varepsilon_\theta} d\varepsilon_\theta$$

$$e^{-2\varepsilon_\theta} = 1 + \sum_{i=1}^{\infty} \frac{(-2)^i (\varepsilon_\theta)^i}{i!}$$

$$V_L = \frac{(t_0)^2 K\beta^{n+1}}{p\mu} \int_{\varepsilon_N}^{\varepsilon_Q} n \varepsilon_\theta^{n-1} \left[1 + \sum_{i=1}^{\infty} \frac{(-2)^i (\varepsilon_\theta)^i}{i!} \right] d\varepsilon_\theta$$

$$V_L = \frac{(t_0)^2 K\beta^{n+1}}{p\mu} \int_{\varepsilon_N}^{\varepsilon_Q} \left[n \varepsilon_\theta^{n-1} + \sum_{i=1}^{\infty} \frac{(-2)^i}{i!} n (\varepsilon_\theta)^{i+n-1} \right] d\varepsilon_\theta$$

$$V_L = \frac{(t_0)^2 K\beta^{n+1}}{p\mu}$$

$$\times \left\{ (\varepsilon_Q^n - \varepsilon_N^n) + \sum_{i=1}^{\infty} \frac{(-2)^i}{i!} \frac{n}{n+i} (\varepsilon_Q^{n+i} - \varepsilon_N^{n+i}) \right\} \tag{51}$$

The volume of the free expansion section can be calculated as

$$V_F = \int_0^{SF} t \, ds$$

$$= \int_0^{SF} t_0 e^{-\varepsilon_\theta} \, ds$$

$$= \int_0^{SF} t_0 e^{-\varepsilon_Q} \, ds \tag{52}$$

SF is the arc length of the free expansion section, shown in Fig. 7 which can be calculated as follows

$$SF = rr \times \varphi$$

$$= (r - Lctg(\pi - \alpha))\varphi$$

$$= (r - Lctg(\pi - \alpha))(\pi - \alpha) \tag{53}$$

Substituting equation (53) into equation (52)

$$V_F = \int_0^{SF} t_0 e^{-\varepsilon_Q} \, ds$$

$$= t_0 e^{-\varepsilon_Q} SF$$

$$= (r - Lctg(\pi - \alpha))(\pi - \alpha) t_0 e^{-\varepsilon_Q} \tag{54}$$

The sum of the volumes of the three sections equals the volume of the deformed tube, as depicted in equation (55). By substituting equations (50), (51), and (54) into equation (55), equation (56) can be obtained

$$V = V_C + V_L + V_F \tag{55}$$

$$V = \pi r t_0 = \int_0^{\alpha} r t_0$$

$$e^{-\left(\left\{\varepsilon_N^n - \left[(\lambda-1)p/K\beta^{n+1}\right]\right\} e^{\mu(\theta-\alpha)} + \left[(\lambda-1)p/K\beta^{n+1}\right]\right)^{1/n}} d\theta$$

$$+ \frac{(t_0)^2 K\beta^{n+1}}{p\mu} \left\{ (\varepsilon_Q^n - \varepsilon_N^n) + \sum_{i=1}^{\infty} \frac{(-2)^i}{i!} \frac{n}{n+i} (\varepsilon_Q^{n+i} - \varepsilon_N^{n+i}) \right\}$$

$$+ (r - Lctg(\pi - \alpha))(\pi - \alpha) t_0 e^{-\varepsilon_Q} \tag{56}$$

In equation (56), if K, n, p, μ, r, t_0, L, α are known there will be two unknown variables ε_N and ε_Q. To solve these two variables equation (45) and equation (56) are used as shown in group equation (57)

$$\begin{cases} \pi r t_0 = \int_0^{\alpha} r t_0 \\ \quad e^{-\left(\left\{\varepsilon_N^n - \left[(\lambda-1)p/K\beta^{n+1}\right]\right\} e^{\mu(\theta-\alpha)} + \left[(\lambda-1)p/K\beta^{n+1}\right]\right)^{1/n}} d\theta \\ \quad + \frac{(t_0)^2 K\beta^{n+1}}{p\mu} \left\{ (\varepsilon_Q^n - \varepsilon_N^n) + \sum_{i=1}^{\infty} \frac{(-2)^i}{i!} \frac{n}{n+i} (\varepsilon_Q^{n+i} - \varepsilon_N^{n+i}) \right\} \\ \quad + (r - Lctg(\pi - \alpha))(\pi - \alpha) t_0 e^{-\varepsilon_Q} \\ \frac{1}{n}(\varepsilon_Q^n - \varepsilon_N^n) + \sum_{i=1}^{\infty} \frac{(-1)^i}{i!} \frac{1}{i+n} (\varepsilon_Q^{i+n} - \varepsilon_N^{i+n}) = \frac{\mu p}{K\beta^{n+1} n t_0} L \end{cases} \tag{57}$$

Equation (57) can be solved for ε_N and ε_Q using the Newton–Raphson method. The solution scheme is given in Appendix 3.

4.2 Pressure prediction

The above analysis of stress and strain is based on knowing the pressure. Thus a method to predict the

required pressure needs to be established when the deformation of the tube is known. In fact, the deformed shape of the tube can be determined by the parameter L. From equation (46), hoop stress in free expansion can be expressed by the following equation

$$\sigma_\theta = K\beta^{n+1}\varepsilon_Q^n \tag{58}$$

Hoop stress can also be calculated by the equilibrium equation in the radial direction (Refer to Fig. 6), as given in equation (59)

$$\sigma_\theta t - prr = 0 \Rightarrow \sigma_\theta = \frac{rr}{t}p \tag{59}$$

$$t = t_0 e^{-\varepsilon_Q} \tag{60}$$

Substituting equations (58) and (60) into equation (59), an expression for pressure p, can be obtained as given in equation (61)

$$p = \frac{K\beta^{n+1}\varepsilon_Q^n t_0 e^{-\varepsilon_Q}}{rr} \tag{61}$$

$$rr = r - Lctg(\pi - \alpha)$$

$$p = \frac{K\beta^{n+1}\varepsilon_Q^n t_0 e^{-\varepsilon_Q}}{r - Lctg(\pi - \alpha)} \tag{62}$$

Equation (62) can be combined with equation (58) to form group equation (63). From equation (63) ε_N, ε_Q, and p can be solved provided K, n, p, μ, r, t_0, L, α are known quantities

$$\begin{cases}
\pi r t_0 = \int_0^\alpha r t_0 \\
\quad e^{-\left(\left\{\varepsilon_N^n - [(\lambda-1)p/K\beta^{n+1}]\right\}e^{\mu(\theta-\alpha)} + [(\lambda-1)p/K\beta^{n+1}]\right)^{1/n}}d\theta \\
\quad + \dfrac{(t_0)^2 K\beta^{n+1}}{p\mu}\left\{(\varepsilon_Q^n - \varepsilon_N^n) + \sum_{i=1}^\infty \dfrac{(-2)^i}{i!}\dfrac{n}{n+i}(\varepsilon_Q^{n+i} - \varepsilon_N^{n+i})\right\} \\
\quad\quad + (r - Lctg(\pi-\alpha))(\pi-\alpha)t_0 e^{-\varepsilon_Q} \\
\dfrac{\mu p}{K\beta^{n+1}n t_0}L = \frac{1}{n}(\varepsilon_Q^n - \varepsilon_N^n) + \sum_{i=1}^\infty \dfrac{(-1)^i}{i!}\dfrac{1}{i+n}(\varepsilon_Q^{i+n} - \varepsilon_N^{i+n}) \\
\quad\quad p = \dfrac{K\beta^{n+1}\varepsilon_Q^n t_0 e^{-\varepsilon_Q}}{r - Lctg(\pi-\alpha)}
\end{cases} \tag{63}$$

Equation (63) is non-linear; therefore, pressure P is solved by using the Newton–Raphson. The solution scheme is given in Appendix 3.

5 RESULTS AND DISCUSSION

5.1 Comparison between analytical model and finite element simulation results

Finite element simulations of the pear-shaped tribotest were carried out to validate the closed-form

solutions developed for radial stress, longitudinal stress, hoop stress, effective stress and strain, longitudinal strain, and radial strain given in equations (30), (43), and (46) for the arc, linear, and free sections, respectively, and the solutions for pressure prediction given in equation (63). The finite element simulations were carried out by commercial software, DEFORM 2D. Various case studies were simulated, a subset of which is presented in this paper. Table 1 shows variables used for model validation. The model contained a total of 1000 elements, 5 elements being across the wall thickness. Figures 8 and 9 show the contact pressure, effective stress, effective strain, and predicted pressure from FEA and the analytical model. Figure 8 shows results for $\mu = 0.05$, and Fig. 9 for $\mu = 0.15$. There is good agreement between model and FEA, particularly, for the linear and expansion sections. The model slightly over predicts the contact pressure in the arc section. Note: The curvilinear length shown in the x-axes represents the length from the arc section of the pear tube (point A) to the free expansion section, point B (Table 1).
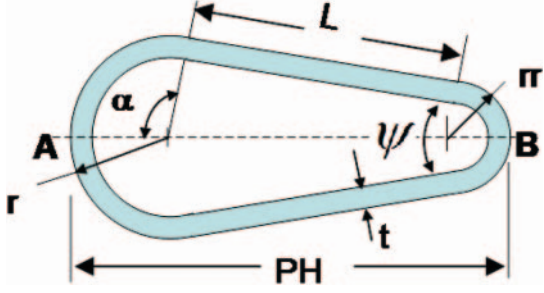
5.2 Potential applications of the developed closed-form solutions

The established closed-form solution can be used as a quick tool for studying field variables for THF parts with geometrical configuration similar to pear shaped. For instance, the interface pressure distribution at the die-wall interface shown in Figs 8(a) and 9(a) demonstrates that with complex die geometry, the interface pressure can vary drastically from one region to the other. Figure 8(a) shows that for an internal fluid pressure Pi of 30 MPa, the pressure at the die-wall interface varied from 12 MPa to 32 MPa. This high-pressure gradient provides an insight into the tribological conditions inherent in the process. As discussed in section 1, experimental determination of friction coefficient values using the expansion zone tribotest is difficult. The established closed-form solutions provide for a quick way of determining friction coefficient and could be used for optimizing a pear-shaped tribotest. More details on the applications of the analytical model are given in Part 2 of this paper [14].

5.2.1 Prediction of friction coefficient by calibration chart

Having derived the expressions for interface pressure at the arc and linear sections, it is now possible to determine the interface friction. Owing to the complex interaction of variables, the friction coefficient cannot be expressed explicitly. Thus, friction calibration charts are constructed. These charts can be used to estimate friction coefficient of the lubricant tested

Table 1 Variables for model validation

Material parameters:

$K = 500\,\text{MPa}, \ n = 0.5$

Geometric parameters:

$L_1 = 50\,\text{mm}, \ L_2 = 46\,\text{mm}, \ \text{PH}_1 = 136\,\text{mm},$

$\text{PH}_2 = 132\,\text{mm}, \ r = 50\,\text{mm}, \ t = 4\,\text{mm}, \ \alpha = 110°$

Process parameters

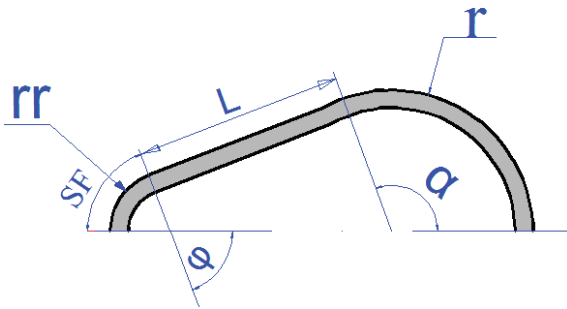$\mu_1 = 0.05, \ \mu_2 = 0.15, \ Pi = 30\,\text{MPa}$

Fig. 7 Free expansion section of tube

using the pear-shaped tribotest. The four equations used to establish the calibration curves are based on volume constancy, pressure prediction, and geometric relationship between L and PH.

1. Volume constant equation recapitulated from equation (57) can be rearranged into equation (64)

$$
\begin{cases}
\pi r t_0 = \int_0^\alpha r t_0 \\
\times \mathrm{e}^{-\left(\left\{\varepsilon_N^n - \left[(\lambda-1)p/K\beta^{n+1}\right]\right\}\mathrm{e}^{\mu(\theta-\alpha)} + \left[(\lambda-1)p/K\beta^{n+1}\right]\right)^{1/n}} \mathrm{d}\theta \\
\quad + \dfrac{1}{p/K}\dfrac{(t_0)^2\beta^{n+1}}{\mu}\left\{(\varepsilon_Q^n - \varepsilon_N^n) + \sum_{i=1}^{\infty}\dfrac{(-2)^i}{i!}\dfrac{n}{n+i}(\varepsilon_Q^{n+i} - \varepsilon_N^{n+i})\right\} \\
\qquad + (r - Lctg(\pi-\alpha))(\pi-\alpha)t_0 \mathrm{e}^{-\varepsilon_Q} \\
\dfrac{1}{n}(\varepsilon_Q^n - \varepsilon_N^n) + \sum_{i=1}^{\infty}\dfrac{(-1)^i}{i!}\dfrac{1}{i+n}(\varepsilon_Q^{i+n} - \varepsilon_N^{i+n}) = \dfrac{\mu L}{\beta^{n+1}nt_0}p/k
\end{cases}
$$
(64)

2. Pressure prediction equation recapitulated from equation (62) can be rearranged into equation (65), which represents a normalized pressure with material strength coefficient K

$$p/k = \frac{\beta^{n+1}\varepsilon_Q^n t_0 \mathrm{e}^{-\varepsilon_Q}}{r - Lctg(\pi-\alpha)}$$
(65)

3. Geometrical relationship between L and H

Figure 10 shows the geometric parameters for the pear-shaped tube. By trigonometric manipulation, equations (66) and (67) can be obtained

$$rr = r - Lctg(\pi - \alpha)$$
(66)

$$L = \frac{\text{PH} - 2r}{\csc(\pi - \alpha) - ctg(\pi - \alpha)}$$
(67)

Combining equations (64), (65), (66), and (67), equation group (68) can be obtained

$$
\begin{cases}
\pi r t_0 = \int_0^\alpha r t_0 \\
\quad \times \mathrm{e}^{-\left(\left\{\varepsilon_N^n - \left[(\lambda-1)/\beta^{n+1}\right]p/k\right\}\mathrm{e}^{\mu(\theta-\alpha)} + \left[(\lambda-1)/\beta^{n+1}\right]p/k\right)^{1/n}} \mathrm{d}\theta \\
\quad + \dfrac{1}{p/K}\dfrac{(t_0)^2\beta^{n+1}}{\mu}\left\{(\varepsilon_Q^n - \varepsilon_N^n) + \sum_{i=1}^{\infty}\dfrac{(-2)^i}{i!}\dfrac{n}{n+i}(\varepsilon_Q^{n+i} - \varepsilon_N^{n+i})\right\} \\
\qquad + (r - Lctg(\pi-\alpha))(\pi-\alpha)t_0 \mathrm{e}^{-\varepsilon_Q} \\
\dfrac{p}{K}\dfrac{\mu}{\beta^{n+1}nt_0}L = \dfrac{1}{n}(\varepsilon_Q^n - \varepsilon_N^n) + \sum_{i=1}^{\infty}\dfrac{(-1)^i}{i!}\dfrac{1}{i+n}(\varepsilon_Q^{i+n} - \varepsilon_N^{i+n}) \\
\dfrac{p}{K} = \dfrac{\beta^{n+1}\varepsilon_Q^n t_0 \mathrm{e}^{-\varepsilon_Q}}{r - Lctg(\pi-\alpha)} \\
L = \dfrac{\text{PH} - 2r}{\csc(\pi-\alpha) - ctg(\pi-\alpha)}
\end{cases}
$$
(68)

In equation group (68), if dimensions r, t, and α and material properties K and n are known, then there will be six unknown variables: PH, L, p, μ, ε_N, and ε_Q. Because the internal pressure Pi and protrusion height PH can be obtained from experiment, the unknown variables in equation (68) are L, μ, ε_N, and ε_Q. Thus, equation group (68) can be solved to obtain μ. However, μ cannot be determined explicitly; therefore calibration chart is used to estimate μ. The calibration chart is composed of a family of curves (PH versus p/K) for different friction coefficient values. Figure 11 shows an example of a friction calibration chart for a pear-shaped expansion test for tube material whose flow stress follows power law ($\overline{\sigma} = K\overline{\varepsilon}^n$), where $n = 0.52$, $r = 17.46$ mm, $t = 1.24$ mm, and die vertex angle, $\psi = 48°$. By superimposing on a graph the normalized internal pressure (p/K) and protrusion height PH measured from a pear-shaped tube, the
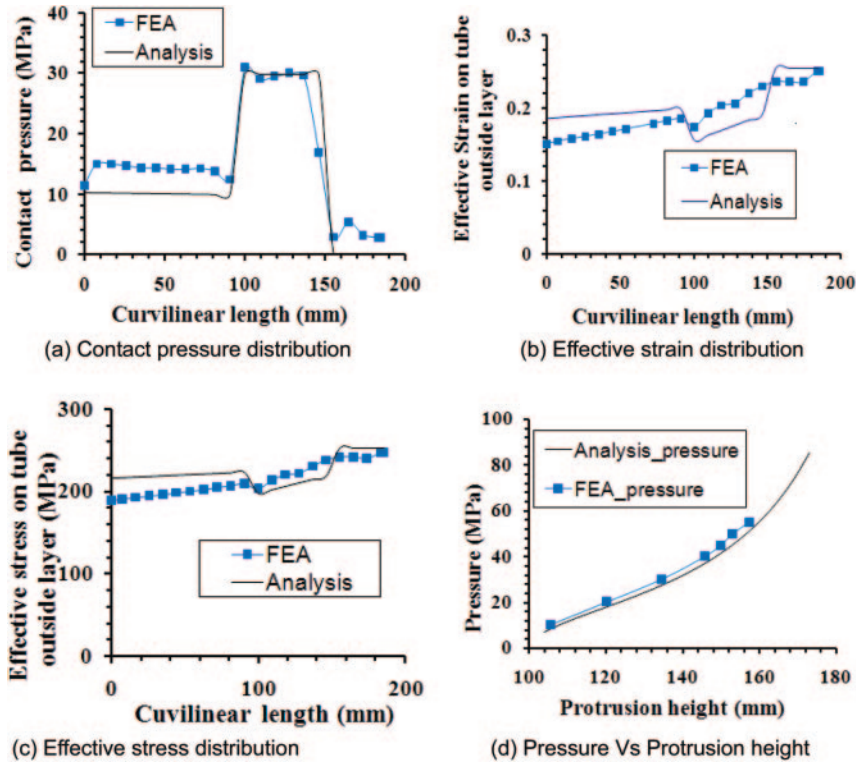
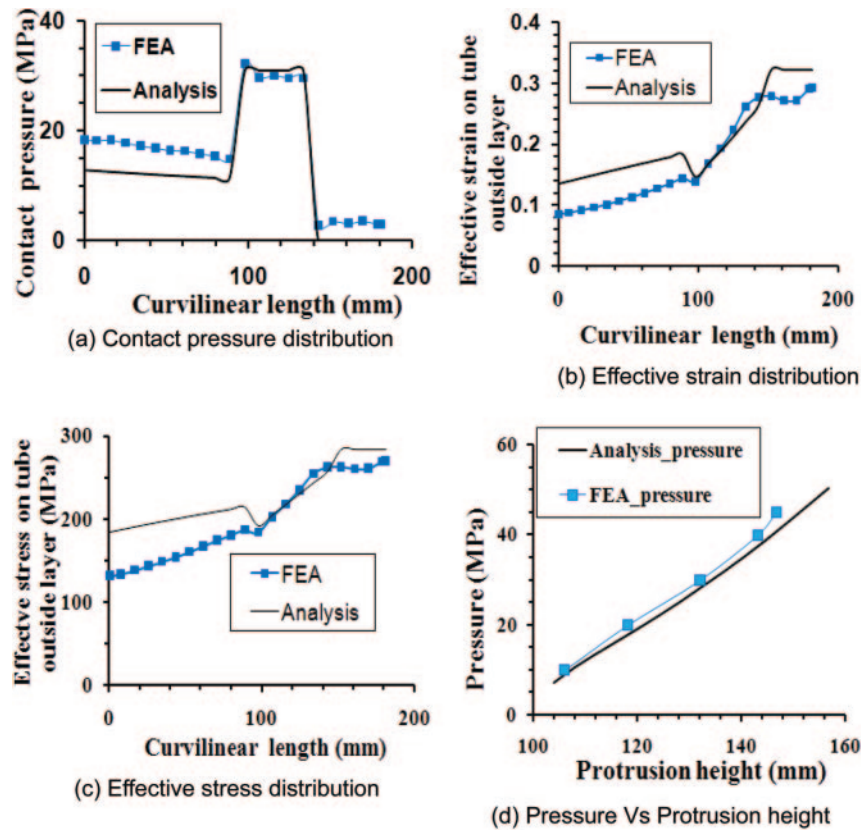**Fig. 8** Analytical model and FEA; comparison of various field variables for $\mu = 0.05$

Fig. 9 Analytical model and FEA; comparison of various field variables for $\mu = 0.15$
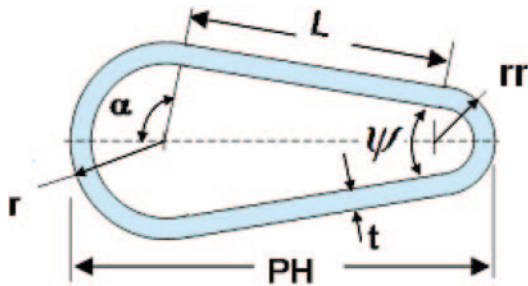
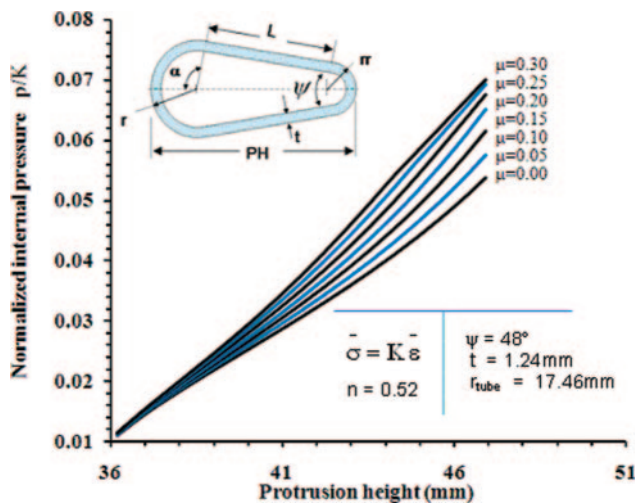**Fig. 10** Geometric parameters for pear-shaped expanded tube

Fig. 11 Friction calibration chart

friction coefficient for a tested lubricant can be determined. Note that the friction calibration chart is dependent on strain hardening exponent of material, n, die geometry, and tube size. Part 2 of this paper presents a case study where friction coefficients for two lubricants were determined [**14**].

6 CONCLUSIONS

Closed-form solutions that characterize the pear-shaped tribotest for tube hydroforming were established based on a mechanistic approach. The analytical model makes possible the computation of field variables as a function of friction coefficient, fluid pressure, and strain hardening exponent of material. The variables that can be computed from the equations are (a) contact pressure distribution, (b) effective stress and strain distribution, (c) longitudinal stress and strain distribution, and (d) hoop stress distribution. The model also provides for determining the coefficient of friction via friction calibration curves.

As well as facilitating the determination of friction coefficient for tested lubricants, the analytical model can be used as a tool in rapid optimization of pear-shaped tribotest conditions. For a predetermined test pressure band, pear-shaped die geometry can be optimized to suit type of tubular materials to be tested and tube sizes.

ACKNOWLEDGEMENT

REFERENCES

1 Koc, M. and **Altan, T.** An overall review of the tube hydroforming (THF) technology. *J. Mater. Process. Technol.*, 2001, **108**, 384–393.

2 Siegert, K., Häussermann, M., Lösch, B., and **Rieger, R.** Recent developments in hydroforming technology. *J. Mater. Process. Technol.*, 2000, **98**, 251–258.

3 Vollersten, F. and **Plancak, M.** On possibilities for the determination of the coefficient of friction in hydroforming of tubes. *J. Mater. Process. Technol.*, 2002, **125–126**, 412–420.

4 Nguyen, B. N., Johson, K., and **Khaleel, M. A.** Analysis of tube hydroforming by means of an inverse approach 1. *J. Mfg Sci. Engng*, 2003, **125**, 369–377.

5 Dohmann, F. and **Hartl, Ch.** Hydroforming – a method to manufacture lightweight parts. *J. Mater. Process. Technol.*, 1996, **60**, 669–676.

6 Asnafi, N. and **Skogsgårdh, A.** Theoretical and experimental analysis of stroke-controlled tube hydroforming. *Mater. Sci. Engng A*, 2000, **279**(1–2), 95–110.

7 Osen, W. *Specific design concepts for hydroforming presses*, 1999, pp. 139–148 (MAT-INFO Werksstoff-Informationosgesellschaft mbH, Frankfurt).

8 Ngaile, G., Jaeger, S., and **Altan, T.** Lubrication in tube hydroforming (THF). Part I: lubrication mechanisms and development of model tests to evaluate lubricants and die coatings in the transition and expansion zones. *J. Mater. Process. Technol.*, 2004, **146**, 108–115.

9 Prier, M. and **Schmoeckel, D.** Tribology of internal high pressure forming, 1999, pp. 379–390 (MAT-INFO Werksstoff-Informationosgesellschaft mbH, Frankfurt).

10 Ngaile, G. and **Altan, T.** Practical methods for evaluation lubricants for tube hydroforming. *Hydroforming J.*, 2001, 8–12.

11 Dalton, G. The role of lubricants in hydroforming. In *Proceedings of the Automotive Tube Conference*, Dearborn, MI, 26–27 April 1999.

12 Ngaile, G., Jaeger, S., and **Altan, T.** Lubrication in tube hydroforming (THF). Part II: performance evaluation of lubricants using LDH test and pear shaped tube expansion test. *J. Mater. Process. Technol.*, 2004, **146**, 116–123.

13 Imaninejad, M. and **Subhash, G.** Proportional loading of thick-walled cylinders. *Int. J. of Pressure Vessels Piping*, 2005, **82**, 129–135.

14 **Ngaile, G.** and **Yang, C.** Applications of analytical model for characterizing the pear-shaped tribotest for tube hydroforming. Part 2. *Proc. IMechE, Part B. J. Engineering Manufacture*, 2008, **222**(B7), 865–886.

APPENDIX 1

Notation

K	strength coefficient
L	linear section length
n	strain hardening exponent
PH	protrusion height of deformed tube
Pi/p	internal pressure
r	outer radius of tube
rr	corner radius of tube
t	deformed tube thickness
t_0	initial tube thickness
V_C	volume of tube in arc section
V_F	volume of tube in free expansion section
V_L	volume of tube in linear section
α	centre angle of arc section
$\bar{\varepsilon}$	effective strain
ε_N	hoop strain at the intersection between arc and linear sections
ε_Q	hoop strain at the free expansion zone
ε_r	radial strain
ε_z	longitudinal strain
ε_θ	hoop strain
λ	ratio of outer radius to tube thickness
μ	friction coefficient
$\bar{\sigma}$	effective stress
σ_r	radial stress
σ_z	longitudinal stress
σ_θ	hoop stress
ϕ	centre angle of free expansion section
ψ	vertex pear-shaped die angle

APPENDIX 2: STRESS AND STRAIN ANALYSIS IN THE OUTSIDE AND INSIDE TUBE LAYERS

Linear section

In the linear section, the tube is experiencing stretching and bending. The inside layer is stretched while the outside layer is compressed. The strain and stress in the inside and outside layers can be determined based on the calculated hoop strain in the middle layer as illustrated below. Figure 12 shows how bending evolves in the linear section.

From Fig. 12 equation (69) can be obtained

$$\begin{aligned}
\varepsilon_{\theta,i} &= \ln\left(\frac{Ln'}{Li}\right) = \ln\left(\frac{e^{\varepsilon_\theta}Ln}{Li}\right) = \ln(e^{\varepsilon_\theta}) + \ln\left(\frac{Ln}{Li}\right) \\
&= \varepsilon_\theta + \ln\left[\frac{Rn}{(Rn - t_0/2)}\right] \varepsilon_{\theta,o} = ln\left(\frac{Ln'}{Lo}\right) \\
&= \ln\left(\frac{e^{\varepsilon_\theta}Ln}{Lo}\right) = \ln(e^{\varepsilon_\theta}) + \ln\left(\frac{Ln}{Lo}\right) \\
&= \varepsilon_\theta + \ln\left[\frac{Rn}{(Rn + t_0/2)}\right]
\end{aligned}$$

$$(69)$$

$$Rn = r - t_0/2$$

$$\begin{aligned}
\varepsilon_{\theta,i} &= \varepsilon_\theta + \ln\left(\frac{r - t_0/2}{r - t_0}\right) = \varepsilon_\theta + \ln\left(1 + \frac{t_0/2}{r - t_0}\right) \\
\varepsilon_{\theta,o} &= \varepsilon_\theta + \ln\left(\frac{r - t_0/2}{r}\right) = \varepsilon_\theta + \ln\left(1 - \frac{t_0/2}{r}\right)
\end{aligned}$$

$$(70)$$

The hoop strain in outside and inside layers $\varepsilon_{\theta,o}$, $\varepsilon_{\theta,i}$ can be calculated from equation (70) if the average hoop strain ε_θ is known. Since other state variables are based on the hoop strain, knowing $\varepsilon_{\theta,o}$ and $\varepsilon_{\theta,i}$ implies that other state variables for the inside and outside layers can be determined. Note that the average strain for the arc, linear, and free expansion sections are determined by equations (30), (43), and (46).

Free expansion section

In the free expansion section, the tube is also experiencing stretching and bending. The inside layer is compressed while the outside layer is stretched relative to the middle layer. The strain and stress in the inside and outside layers can be determined based on the calculated hoop strain in the middle layer as illustrated below
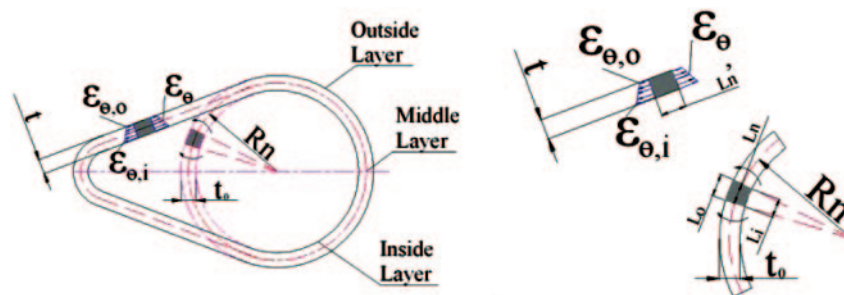

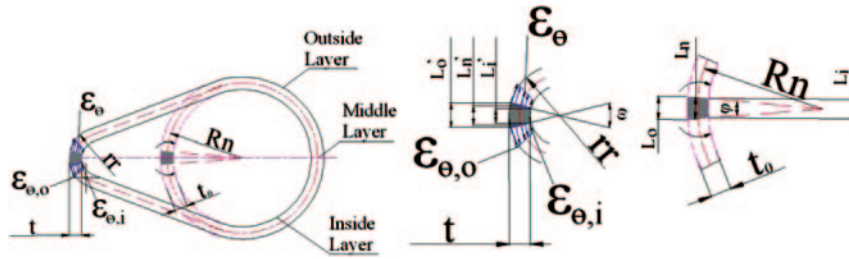**Fig. 12**   Bending in the linear section

Fig. 13 Bending in the free expansion section

$$
\begin{aligned}
\varepsilon_{\theta,\mathrm{i}} &= & \ln\left(\frac{Li'}{Li}\right) = \ln\left\{\frac{(rr-t)\omega}{[(Rn-t_0/2)\varphi]}\right\} \\
&= & \ln\left\{\frac{(rr-t)[Ln'/(rr-t/2)]}{(Rn-t_0/2)\varphi}\right\} = \ln\left\{\frac{(rr-t)\left[Ln\mathrm{e}^{\varepsilon_\theta}/(rr-t/2)\right]}{(Rn-t_0/2)\varphi}\right\} \\
&= & \ln\left\{\frac{(rr-t)\left[\mathrm{e}^{\varepsilon_\theta} Rn\varphi/(rr-t/2)\right]}{(Rn-t_0/2)\varphi}\right\} = \ln\left\{\frac{\left[(rr-t)\left[\mathrm{e}^{\varepsilon_\theta} Rn/(rr-t/2)\right]\right]}{(Rn-t_0/2)}\right\} \\
&= & \ln\left[\frac{(rr-t)}{(rr-t/2)}\mathrm{e}^{\varepsilon_\theta}\frac{Rn}{(Rn-t_0/2)}\right] \\
&= & \varepsilon_\theta + \ln\left[\frac{(rr-t)}{(rr-t/2)}\frac{Rn}{(Rn-t_0/2)}\right] \\
&= & \varepsilon_\theta + \ln\left[\frac{rr-t}{rr-t/2}\right] + \ln\left[\frac{Rn}{Rn-t_0/2}\right] \\
&= & \varepsilon_\theta + \ln\left[\frac{rr-t_0\mathrm{e}^{\varepsilon_\theta}}{(rr-t_0\mathrm{e}^{\varepsilon_\theta}/2)}\right] + \ln\left[\frac{(r-t_0/2)}{r-t_0}\right]
\end{aligned}
$$

$$
\begin{aligned}
\varepsilon_{\theta,\mathrm{o}} &= & \ln\left(\frac{Lo'}{Lo}\right) = \ln\left\{\frac{rr\omega}{[(Rn+t_0/2)\varphi]}\right\} \\
&= & \ln\left\{\frac{rr[Ln'/(rr-t/2)]}{(Rn+t_0/2)\varphi}\right\} = \ln\left\{\frac{rr\left[Ln\mathrm{e}^{\varepsilon_\theta}/(rr-t/2)\right]}{(Rn-t_0/2)\varphi}\right\} \\
&= & \ln\left\{\frac{rr\left[(\mathrm{e}^{\varepsilon_\theta} Rn\varphi)/(rr-t/2)\right]}{(Rn+t_0/2)\varphi}\right\} = \ln\left\{\frac{rr\left[(\mathrm{e}^{\varepsilon_\theta} Rn)/(rr-t/2)\right]}{(Rn+t_0/2)}\right\} \\
&= & \ln\left[\frac{rr}{(rr-t/2)}\mathrm{e}^{\varepsilon_\theta}\frac{Rn}{(Rn+t_0/2)}\right] \\
&= & \varepsilon_\theta + \ln\left[\frac{rr}{(rr-t/2)}\frac{Rn}{(Rn+t_0/2)}\right] \\
&= & \varepsilon_\theta + \ln\left[\frac{rr}{(rr-t/2)}\right] + \ln\left[\frac{Rn}{(Rn+t_0/2)}\right] \\
&= & \varepsilon_\theta + \ln\left[\frac{rr}{(rr-t_0\mathrm{e}^{\varepsilon_\theta}/2)}\right] + \ln\left[\frac{(r-t_0/2)}{r}\right]
\end{aligned}
$$

$$
\varepsilon_{\theta,\mathrm{i}} = \varepsilon_\theta + \ln\left[\frac{rr - t_0\mathrm{e}^{\varepsilon_\theta}}{(rr - t_0\mathrm{e}^{\varepsilon_\theta}/2)}\right] + \ln\left[\frac{(r - t_0/2)}{r - t_0}\right] \quad (71)
$$

$$
\varepsilon_{\theta,\mathrm{o}} = \varepsilon_\theta + \ln\left[\frac{rr}{(rr - t_0\mathrm{e}^{\varepsilon_\theta}/2)}\right] + \ln\left[\frac{(r - t_0/2)}{r}\right] \quad (72)
$$

The hoop strain in outside and inside layers $\varepsilon_{\theta,\mathrm{o}}$, $\varepsilon_{\theta,\mathrm{i}}$ can be calculated from the above equations if the average hoop strain ε_θ is known. Similarly, if $\varepsilon_{\theta,\mathrm{o}}$ and $\varepsilon_{\theta,\mathrm{i}}$ are known all other state variables for the inside and outside layers can be determined.

APPENDIX 3: SOLUTION SCHEME FOR EQUATION (63)

The Newton–Raphson Method is used to solve non-linear equation (63) in the following steps.

1. Reform equation (63) into equation (73)

$$
F = \left\{\begin{array}{c} f_1 \\ f_2 \\ f_3 \end{array}\right\} = \left\{\begin{array}{l}
f_1(p, \varepsilon_\mathrm{N}, \varepsilon_\mathrm{Q}) = \int_0^\alpha rt_0 \mathrm{e}^{-\left(\left\{\varepsilon_\mathrm{N}^n - \left[\frac{(\lambda-1)p}{(K\beta^{n+1})}\right]\right\}\mathrm{e}^{\mu(\theta-\alpha)} + \left[\frac{(\lambda-1)p}{(K\beta^{n+1})}\right]\right)^{1/n}} \mathrm{d}\theta \\
\qquad + \frac{(t_0)^2 K\beta^{n+1}}{p\mu}\left[(\varepsilon_\mathrm{Q}^n - \varepsilon_\mathrm{N}^n) + \sum_{i=1}^\infty \frac{(-2)^i}{i!}\frac{n}{n+i}(\varepsilon_\mathrm{Q}^{n+i} - \varepsilon_\mathrm{N}^{n+i})\right] \\
\qquad + (r - L\,ctg(\pi - \alpha))(\pi - \alpha)t_0\mathrm{e}^{-\varepsilon_Q} - \pi r t_0 \\
f_2(p, \varepsilon_\mathrm{N}, \varepsilon_\mathrm{Q}) = \frac{1}{n}(\varepsilon_\mathrm{Q}^n - \varepsilon_\mathrm{N}^n) + \sum_{i=1}^\infty \frac{(-1)^i}{i!}\frac{1}{i+n}(\varepsilon_\mathrm{Q}^{i+n} - \varepsilon_\mathrm{N}^{i+n}) - \frac{\mu p}{K\beta^{n+1} n t_0}L \\
f_3(p, \varepsilon_\mathrm{Q}) = \frac{K\beta^{n+1}\varepsilon_\mathrm{Q}^n t_0\mathrm{e}^{-\varepsilon_Q}}{r - L\,ctg(\pi - \alpha)} - p
\end{array}\right.
$$

$$(73)$$

2. Obtain the Jacobian matrix of F

$$Df(p, \varepsilon_{\mathrm{N}}, \varepsilon_{\mathrm{Q}}) = \begin{bmatrix} \dfrac{\partial f_1}{\partial p} & \dfrac{\partial f_1}{\partial \varepsilon_{\mathrm{N}}} & \dfrac{\partial f_1}{\partial \varepsilon_{\mathrm{Q}}} \\[2mm] \dfrac{\partial f_2}{\partial p} & \dfrac{\partial f_2}{\partial \varepsilon_{\mathrm{N}}} & \dfrac{\partial f_2}{\partial \varepsilon_{\mathrm{Q}}} \\[2mm] \dfrac{\partial f_3}{\partial p} & \dfrac{\partial f_3}{\partial \varepsilon_{\mathrm{N}}} & \dfrac{\partial f_3}{\partial \varepsilon_{\mathrm{Q}}} \end{bmatrix} \qquad (74)$$

3. Provide initial guess to three unknown variables p, ε_{N}, ε_{Q}

4. Obtain p, ε_{N}, ε_{Q} by iterations as shown in equation (75)

$$\begin{bmatrix} p \\ \varepsilon_{\mathrm{N}} \\ \varepsilon_{\mathrm{Q}} \end{bmatrix}_{k+1} = \begin{bmatrix} p \\ \varepsilon_{\mathrm{N}} \\ \varepsilon_{\mathrm{Q}} \end{bmatrix}_{k} - \left[Df(p, \varepsilon_{\mathrm{N}}, \varepsilon_{\mathrm{Q}})\right]_{k}^{-1} \begin{bmatrix} p \\ \varepsilon_{\mathrm{N}} \\ \varepsilon_{\mathrm{Q}} \end{bmatrix}_{k}$$

$$(75)$$

5. When $||F|| < error$ the iteration stops
    Remarks. Poor initial guess for the three variables may result in divergence. Alternatively, equation (63) could be solved by using Newton–Raphson method by giving initial guess to one variable, preferably ε_{N} and iterate to obtain the other variables.